# Flow rate through microfilters: Influence of the pore size distribution, hydrodynamic interactions, wall slip, and inertia

Kaare H. Jensen, André X. C. N. Valente, and Howard A. Stone

Citation: Physics of Fluids (1994-present) **26**, 052004 (2014); doi: 10.1063/1.4876937
View online: http://dx.doi.org/10.1063/1.4876937
View Table of Contents: http://scitation.aip.org/content/aip/journal/pof2/26/5?ver=pdfcov
Published by the AIP Publishing



PHYSICS OF FLUIDS **26**, 052004 (2014)

# Flow rate through microfilters: Influence of the pore size distribution, hydrodynamic interactions, wall slip, and inertia

Kaare H. Jensen,[1,2,a)] André X. C. N. Valente,[3,4,5] and Howard A. Stone[6,b)]
[1]*Department of Organismic and Evolutionary Biology, Harvard University, Cambridge, Massachusetts 02138, USA*
[2]*Department of Physics, Technical University of Denmark, Kongens Lyngby, DK-2800, Denmark*
[3]*Biocant Biotechnology Innovation Center, Cantanhede, Portugal*
[4]*Center for Neuroscience and Cell Biology, University of Coimbra, Coimbra, Portugal*
[5]*Institute of Fundamental Medicine and Biology, Kazan Federal University, Kazan, Russia*
[6]*Department of Mechanical and Aerospace Engineering, Princeton University, Princeton, New Jersey 08544, USA*

(Received 18 November 2013; accepted 17 April 2014; published online 27 May 2014)

We examine the fluid mechanics of viscous flow through filters consisting of perforated thin plates. We classify the effects that contribute to the hydraulic resistance of the filter. Classical analyses assume a single pore size and account only for filter thickness. We extend these results to obtain an analytical formula for the pressure drop across the microfilter versus the flow rate that accounts for the non-uniform distribution of pore sizes, the hydrodynamic interactions between the pores given their layout pattern, and wall slip. Further, we discuss inertial effects and their order of scaling. © *2014 AIP Publishing LLC*. [http://dx.doi.org/10.1063/1.4876937]

## I. INTRODUCTION

Flow through microfilters occurs in numerous biological and industrial fluid transport processes. Man-made examples include filtering of air- or water-borne particles and biological agents.[1–3] Biological microfilters are found, for example, in the phloem and xylem vascular systems of plants, where neighboring cells are separated by planar membranes covered with pores,[4,5] and in cell membranes where flow occurs through aquaporin channels.[6] Figure 1 presents some of these examples as well as a sketch of a model microfilter. Such flow configurations are usually modelled based on classical pressure-driven Stokes flow through a single pore. In this paper, we further consider how (i) hydrodynamic interactions between the pores, (ii) the non-uniformity of pore sizes, and (iii) wall slip affect the pressure drop versus flow rate relationship. Together, these features constitute the major practical factors governing a microfilter operating at low Reynolds numbers. We present a theoretically derived design formula that accounts for all three of these factors. Finally, we give the order of the scaling associated with the small inertial effects and compare it to experimental data derived from the literature.

The flow through a microfilter is induced by applying a pressure drop $\Delta p$ across it. We denote $U$ as the average velocity in a microfilter pore, $a$ the pore radius, $t$ the pore thickness, $\rho$ the fluid density, and $\mu$ the shear viscosity of the fluid (Fig. 1(a)). In typical applications, the Reynolds number, $\mathcal{R}_e = \rho U a/\mu$, is small. For example, in MEMS applications involving filtering of air, typical Reynolds number falls in the range 0.1-20,[7] while in phloem sieve plates $\mathcal{R}_e \approx 10^{-4}$ (see, e.g., Jensen *et al.*[5]). Inertial effects are therefore expected to be small to moderate for microfilter flows. Also, recall that the Mach number $\mathcal{M}_a = U/c$ is defined as the ratio of a typical fluid velocity

a)Electronic mail: khjensen@fysik.dtu.dk
b)Electronic mail: hastone@princeton.edu

 

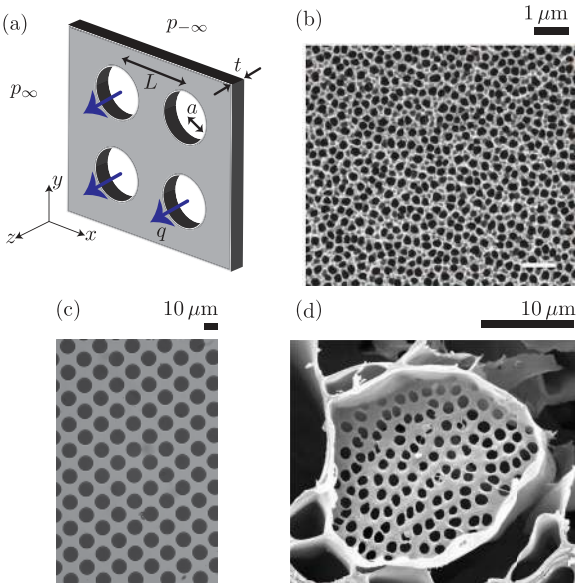


FIG. 1. (a) Sketch of the filter geometry. The flow rate $q$ is driven through pores of radius $a$ by a pressure drop $\Delta p = p_{-\infty} - p_\infty$ across a filter of thickness $t$. The pores are separated by a distance $L$. Examples of man-made and biological microfilters: (b) Carbon nanotube membrane for water desalination and purification.[10] (c) Silicon microfiltration membrane for capture of micron-sized particles.[3] (d) Phloem sieve plate.[5,11] (b) and (c) Reproduced with permission from Yang *et al.*, Nat. Commun. **4**, 2220 (2013). Copyright 2013 Nature Publishing Group and Lin *et al.*, Phys. Fluids **21**, 073301 (2009). Copyright 2009 AIP Publishing LLC. (d) Courtesy of M. Knoblauch and D. L. Mullendore, Washington State University. As originally published in Jensen *et al.*, Front. Plant Sci. **3**, 151 (2012).

to the speed of sound $c$. For viscously dominated flows, compressibility effects are negligible when the square of the Mach number is much smaller than the Reynolds number ($\mathcal{M}_a^2 \ll \mathcal{R}_e$),[8] which is typical for gas flows of interest here. For example, based on the average velocity through a pore, the microfilters of Ho and co-workers[7] for handling gas flows were always used at Mach numbers below 0.2. It is therefore safe to assume compressibility effects are negligible, even for gas flows. We will assume incompressibility of the flow throughout our analysis.[9]

Numerous studies on the topic of filter flow have been performed. In the following we summarize results relevant to the context of our study. More than a century ago, Couette[12] was among the first to discuss viscous dissipation of energy near the orifice of a cylindrical tube. He added a fictitious length to the actual tube length in Poiseuille's formula to account for the pressure drop associated with flow close to the aperture. One year later, in 1891, Sampson[13] published an analytical solution of pressure-driven Stokes flow through a single pore in an infinite plane of zero thickness. Roscoe[14] later corrected a numerical error in Sampson's formula and found solutions for flow through elliptical pores and long slits using an electrostatic analogy. Weissberg[15] and subsequently Dagan *et al.*[16] considered the effects of a finite pore thickness. They showed that the flow can be characterized by a linear superposition of the resistances due to Sampson flow at the aperture and Poiseuille flow inside the pore, in qualitative agreement with the observations by Couette. To account for hydrodynamic interactions, Hasimoto[17] studied flow through an array of parallel slits, and found that interactions among neighboring slits tend to decrease the pressure drop required to drive a given flow. This work was extended by Tio and Sadhal[18] and Wang,[19] who considered hydrodynamic interactions in flows through regular arrays of circular and rectangular pores. Finally, Jensen *et al.*[5] studied the effect of a non-uniform pore size distribution on the flow in biological filters.

We extend these results to obtain a general analytical formula for the pressure drop across a microfilter versus the flow rate, which accounts for pore separation, the geometrical layout of the pores, wall slip, small inertial effects, and a non-uniform distribution of pore sizes. In particular, we go beyond the simple superposition given by Eq. (5) by including the influence of the pore size distribution (see Eq. (9) below) and the interaction between pores (see Eq. (15) below and Appendix A).

## II. THE WEISSBERG-SAMPSON-POISEUILLE APPROXIMATION

We begin our analysis by neglecting all inertial effects and approximating the flow as an incompressible Stokes flow. Sampson[13] solved the problem of Stokes flow through a circular pore in an infinitely thin plate due to a pressure drop applied across the pore. This configuration is shown in Figure 2(a). Above and below the plate, the steady flow satisfies the continuity and Stokes equations,

$$\nabla \cdot \mathbf{v} = 0 \qquad \text{and} \qquad \mu \nabla^2 \mathbf{v} - \nabla p = \mathbf{0}, \tag{1}$$

where $\mathbf{v}(\mathbf{x})$ and $p(\mathbf{x})$ represent, respectively, the steady velocity and pressure fields. The boundary conditions are that (i) the velocity decays uniformly at infinity, (ii) the no-slip condition holds everywhere at the filter $(x - y)$ plane except at the pore, and (iii) the pressure approaches two distinct constants at $+\infty$ and at $-\infty$, hence inducing a flow through the pore. Sampson found the pressure drop $\Delta p = p_{-\infty} - p_{\infty}$ versus flow rate $q$ relationship for a single pore to be[13,20]

$$\frac{\Delta p}{q} = \frac{3\mu}{a^3}. \tag{2}$$

The streamlines are hyperbolae, and at large distances from the aperture the solution becomes identical to that for flow from a point source in a wall.[20] In spherical coordinates (see Fig. 2) the flow is thus purely radial when $\rho \gg a$

$$v_\rho = \frac{a^3 \Delta p}{2\pi \mu \rho^2} \cos^2 \theta, \tag{3a}$$

$$v_\theta = 0. \tag{3b}$$

The flow profile at the aperture ($z = 0$) can be computed directly from Sampson's stream function solution in cylindrical coordinates

$$v_r = 0, \tag{4a}$$

$$v_z = \frac{a \Delta p}{2\pi \mu} \sqrt{1 - \left(\frac{r}{a}\right)^2}. \tag{4b}$$

The relationship between pressure drop and flow rate in Eq. (2) is valid for an infinitely thin plate. In several applications, however, the plate thickness $t$ is comparable to the pore radius $a$. This is the case, for example, in phloem sieve plates where $t/a \simeq 0.5$. For low-Reynolds-number flow through a pore of finite thickness $t$ we can add the pressure drop $8q\mu t/(\pi a^4)$ associated with the Poiseuille flow along the pore (Fig. 2(b)) to the basic Sampson result to obtain the isolated

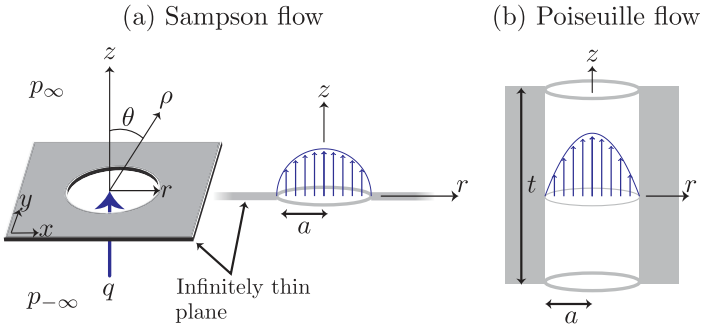


FIG. 2. (a) Sampson flow through a circular pore in an infinitely thin plate. The pore radius is denoted by $a$ and the flow rate by $q$. The pressure drop $\Delta p = p_{-\infty} - p_{\infty}$ is the difference between the pressures at plus and minus infinity. (b) Poiseuille flow along the thickness of a pore. The microfilter thickness is denoted by $t$. At low Reynolds numbers, the simplest result for the ratio of pressure drop to volumetric flow rate per pore is obtained by linearly adding the pressure drops associated with the Sampson and Poiseuille flows.[15,16]

pore-resistance formula

$$\frac{\Delta p}{q} = \frac{3\mu}{a^3} + \frac{8\mu t}{\pi a^4}. \tag{5}$$

This superposition approximation was first proposed by Weissberg[15] and later confirmed by Dagan *et al.*,[16] who showed that the error incurred by linearly adding the Sampson and Poiseuille contributions to the pressure drop is greatest when $t = 2a$, but less than one percent for all values of $t/a$.

From the typical values of $t$ and $a$ in man-made and biological configurations,[7,11] we note that in general both the Sampson and Poiseuille contributions are significant. In Secs. III–VI we address various hydrodynamic and geometric corrections to the basic result given in Eq. (5).

## III. THE INFLUENCE OF A PORE SIZE DISTRIBUTION

In many practical filter applications, the pore radius $a$ in Eq. (5) represents the mean value of a distribution of pore sizes. Here we quantify the effect of a distribution of radii by introducing a distribution function $P(a, \boldsymbol{\sigma})$, where $\boldsymbol{\sigma}$ indicates the parameters describing the distribution. In some cases it is plausible to consider a distribution of pore lengths, but we shall not do this here.

To elucidate how a distribution of pore radii affects the flow rate we begin by considering a finite set of $N$ pores of radius $a_n$, chosen according to the distribution function $P(a, \boldsymbol{\sigma})$. For a parallel coupling of pores, the pressure drop over each pore is identical $\Delta p_n = \Delta p$, while the flow rates $q_n$ add up to the total flow rate $Q = \sum_{n=1}^{N} q_n$. The average pore resistance is therefore

$$\left\langle \frac{\Delta p}{q} \right\rangle = \frac{\Delta p}{Q/N} = \frac{\Delta p}{\frac{1}{N}\sum_{n=1}^{N} q_n}. \tag{6}$$

For sufficiently large values of $N$ we can replace the denominator on the right-hand side of Eq. (6) by its statistical expectation value[21]

$$\frac{1}{N}\sum_{n=1}^{N} q_n = \int q(a) P(a, \boldsymbol{\sigma}) \mathrm{d}a = \langle q \rangle, \tag{7}$$

where the integral goes over all permissible values of the pore radius $a$. Using the expression for the isolated pore resistance in Eq. (5), we now find that the average pore resistance is

$$\left\langle \frac{\Delta p}{q} \right\rangle = 3\mu \left[ \int \left( \frac{1}{a^3} \left[ 1 + \frac{8}{3\pi} \frac{t}{a} \right] \right)^{-1} P(a, \boldsymbol{\sigma}) \mathrm{d}a \right]^{-1}. \tag{8}$$

To simplify Eq. (8) we normalize the pore size $a$ by its average values $\bar{a}$ and introduce the variable $\xi = a/\bar{a}$. With this change of variables we have

$$\left\langle \frac{\Delta p}{q} \right\rangle = \frac{3\mu}{\bar{a}^3} \left[ \int \left( \frac{1}{\xi^3} \left[ 1 + \frac{A}{\xi} \right] \right)^{-1} P(\xi\bar{a}, \boldsymbol{\sigma}) \bar{a} \mathrm{d}\xi \right]^{-1}, \tag{9}$$

where the non-dimensional parameter $A = 8t/(3\pi\bar{a})$ is the ratio of the Poiseuille and Sampson contributions to the pore resistance. In the spirit of the approximations introduced by Weissberg[15] and Dagan *et al.*,[16] we approximate this integral by linearly superposing the limits of a thin pore, $A \ll 1$, and a long pore, $A \gg 1$, which has the form

$$\left\langle \frac{\Delta p}{q} \right\rangle \approx \frac{3\mu}{\bar{a}^3} \left[ \frac{1}{M_3} + \frac{A}{M_4} \right]. \tag{10}$$

Here, $M_3$ and $M_4$ are the third and fourth scaled statistical moments of the distribution $P$[21]

$$M_3 = \int \xi^3 P(\xi\bar{a}, \boldsymbol{\sigma}) \bar{a} \mathrm{d}\xi \qquad \text{and} \qquad M_4 = \int \xi^4 P(\xi\bar{a}, \boldsymbol{\sigma}) \bar{a} \mathrm{d}\xi. \tag{11}$$

TABLE I. Expressions for the probability density function $P(a, \boldsymbol{\sigma})$, the mean pore radius $\bar{a}$, variance $\sigma^2$, and the scaled moments $M_3$ and $M_4$ for five commonly used probability density functions. See, e.g., Rohatgi.[21] The parameters $\boldsymbol{\sigma}$ are defined in column 2, e.g., $\boldsymbol{\sigma} = (m, s)$ for the Log-normal distribution, which represents the mean and standard deviation of the pore radius' natural logarithm. The variance for the Weibull distribution is $H(\lambda, k) = \lambda^2(\Gamma(1 + 2/k) - \Gamma(1 + 1/k)^2)$, where $\Gamma(\cdot)$ is the Gamma function. The exponential distribution is a special case of the Gamma distribution with $\alpha = 1$ and $\beta = \bar{a}$.

| Distribution | $\boldsymbol{\sigma}$ | $P(a, \boldsymbol{\sigma})$ | $\bar{a}$ | $\sigma^2$ | $M_3$ | $M_4$ |
|---|---|---|---|---|---|---|
| Normal | $\bar{a}, \sigma$ | $\frac{1}{\sqrt{2\pi\sigma^2}} \exp\left[-\frac{(\bar{a}-a)^2}{2\sigma^2}\right]$ | $\bar{a}$ | $\sigma^2$ | $1 + 3\left(\frac{\sigma}{\bar{a}}\right)^2$ | $1 + 6\left(\frac{\sigma}{\bar{a}}\right)^2 + 3\left(\frac{\sigma}{\bar{a}}\right)^4$ |
| Log-normal | $m, s$ | $\frac{1}{a\sqrt{2\pi s^2}} \exp\left[-\frac{(\log a - m)^2}{2s^2}\right]$ | $e^{m+s^2/2}$ | $(e^{s^2-1} - 1)e^{2m+s^2}$ | $e^{3s^2}$ | $e^{6s^2}$ |
| Gamma | $\alpha, \beta$ | $\frac{1}{\Gamma(\alpha)\beta^\alpha} a^{\alpha-1} \exp[-a/\beta]$ | $\alpha\beta$ | $\alpha\beta^2$ | $(\alpha + 2)(\alpha + 1)$ | $(\alpha + 3)(\alpha + 2)(\alpha + 1)$ |
| Exponential | $\bar{a}$ | $\frac{1}{\bar{a}} \exp\left[-\frac{a}{\bar{a}}\right]$ | $\bar{a}$ | $\bar{a}^2$ | 6 | 24 |
| Weibull | $\lambda, k$ | $\frac{k}{\lambda}\left(\frac{a}{\lambda}\right)^{k-1} \exp\left[\left(-\frac{a}{\lambda}\right)^k\right]$ | $\lambda\Gamma(1 + 1/k)$ | $H(\lambda, k)$ | $\frac{\Gamma(1+3/k)}{\Gamma(1+1/k)^3}$ | $\frac{\Gamma(1+4/k)}{\Gamma(1+1/k)^4}$ |

Expressions for the moments of five commonly used probability functions are given in Table I. For each of these distributions the average pressure versus flow rate relation can be calculated directly from Eq. (10).

### A. Normally distributed pore radii

We proceed to consider the case of a normal distribution of pore radii in detail. This distribution of pore radii is found, for example, in biological filters such as phloem sieve plates.[5] To quantify the effect of a distribution of radii on the resistance to flow, we keep the average pore radius $\bar{a}$ constant and consider the pressure drop per flow rate as a function of the polydispersity of the pore sizes. A measure of the dispersion is the ratio $B = \sigma/\bar{a}$ of the standard deviation $\sigma$ to the mean pore radius $\bar{a}$. The case $B = 0$ corresponds to a uniform pore size distribution. To elucidate how the pressure drop-flow rate relation is affected by variations in pore size we introduce the function $\gamma$, which is the ratio of resistances with and without a pore size distribution,

$$\gamma(B) = \left\langle \frac{\Delta p}{q} \right\rangle \Big/ \left\langle \frac{\Delta p}{q} \right\rangle_{B=0} \approx \frac{\frac{1}{1+3B^2} + \frac{A}{1+6B^2+3B^4}}{1 + A}, \tag{12}$$

where we have used the expressions for the scaled moments $M_3$ and $M_4$ given in Table I.

The resistance ratio $\gamma$ is plotted as a function of the distribution width $B$ for different values of the pore aspect ratio $A$ in Fig. 3(a). We observe that the influence of the distribution is to diminish the pressure drop required to drive a given flow. For narrow distributions ($B = 0.15$) the required pressure is $5\% - 10\%$ lower, while for broad distributions ($B = 0.5$) $\Delta p$ is reduced by $40\% - 60\%$, indicating that most of the flow is diverted through larger pores. The variability in $\gamma$ for a given value of $B$ is determined by the pore aspect ratio $A$, bounded by the limiting cases of long pores ($A \gg 1$) and thin pores ($A \ll 1$), as indicated in Fig. 3(a). The slope of $\gamma$ (shown in Fig. 3(b)) is most negative in the interval between $B \simeq 0.25$ and $B \simeq 0.33$ indicating that the gain in conductivity diminishes beyond this point. We note that distribution widths observed in phloem sieve plates fall in the range $0.21 < B < 0.34$.[5]

## IV. THE INFLUENCE OF HYDRODYNAMIC INTERACTIONS

### A. A pair of pores

As described above, as a first approximation to flow through a microfilter, the flow through each pore is assumed to be independent. In reality, there exist hydrodynamic interactions between the flow through different pores. These interactions arise due to the pressure field induced by flow through individual pores. In this section, via elementary geometric arguments, we calculate the lowest-order correction to Sampson's single-pore result that accounts for the hydrodynamic interactions between

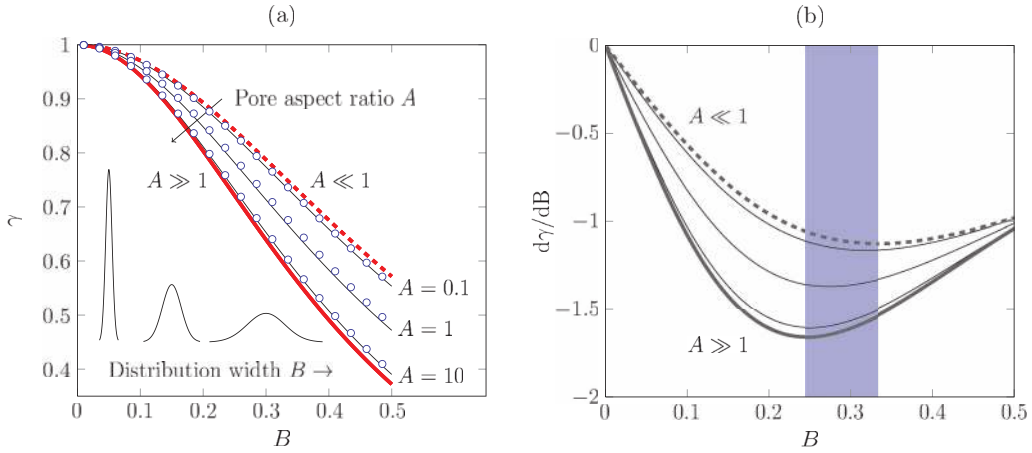


FIG. 3. Effect of pore size distribution on filter resistance. (a) Resistance ratio $\gamma$ plotted as a function of the distribution width $B = \sigma/\bar{a}$ for normally distributed pores. The resistance ratio $\gamma$ was calculated from the approximate result in Eq. (12) (thin lines) and from direct evaluation of the integral in Eq. (9) (circles). Values of the pore aspect ratio $A = 8t/(3\pi\bar{a})$ are indicated in the plot. (b) Slope of the resistance ratio $\mathrm{d}\gamma/\mathrm{dB}$ plotted as a function of the distribution width $B$. Depending on the value of $A$, the slope is most negative in the interval $0.25 < B < 0.33$ (shaded area). In (a) and (b), thick solid and dashed lines show the asymptotic limits for $A \ll 1$ and $A \gg 1$ in Eq. (12).

identical pores. Under certain conditions, our procedure works for pores of different radii, which we discuss briefly in Appendix A. An exact calculation for identical pores with square or hexagonal layouts was given by Tio and Sadhal[18] and Wang,[19] and we compare our approximate results to theirs.

We first treat the case of low-Reynolds-number flow through two adjacent pores in the plane, depicted in Fig. 4. Note that we let the pressures at $\pm\infty$ be anti-symmetric, with the positive pressure being at $-\infty$. Also, the upward volumetric flow rate per pore $q$ is taken as positive. We obtain the lowest-order correction for the change in the flow rate as a function of the non-dimensional relative distance between the pores, $L/a$. Because of the symmetry of the problem: (i) the solution is anti-symmetric about the $x - y$ plane, i.e., $\mathbf{v}(x, y, z) = \big(-v_x(x, y, -z), -v_y(x, y, -z), +v_z(x, y, -z)\big)$ and $p(x, y, z) = -p(x, y, -z)$, (ii) the pressure everywhere at the pore throats equals zero, and (iii) the velocity everywhere at the pore throats is strictly vertical, i.e., $v_x(\mathbf{x}) = v_y(\mathbf{x}) = 0$ at $z = 0$, see Eq. (4b). In view of these symmetries, we need only consider the upper half-plane $z > 0$.

To account for hydrodynamic interactions, and with reference to Fig. 4, we note that adding Sampson's single-pore solution centered about the left pore to Sampson's single-pore solution centered about the right pore does not yield a valid solution to the two-pore problem because each single-pore solution produces a pressure profile at the other pore that violates condition (ii) above. Specifically, for a single open pore, the axisymmetric pressure at the upper side of the $x - y$ plane,

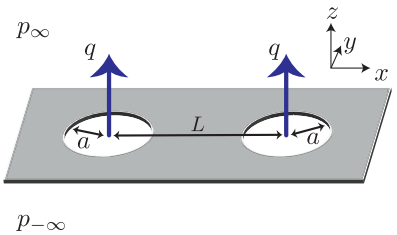


FIG. 4. Pressure-driven flow through two pores in an infinitely thin plane. The hydrodynamic interaction of the flow between the two pores yields a larger flow per pore than that predicted by Sampson's classic result for an isolated pore, under the same pressure drop. The upward flow per pore $q$ is taken as positive. Here $L$ denotes the center-to-center distance between the pores and $a$ denotes the pore radii.

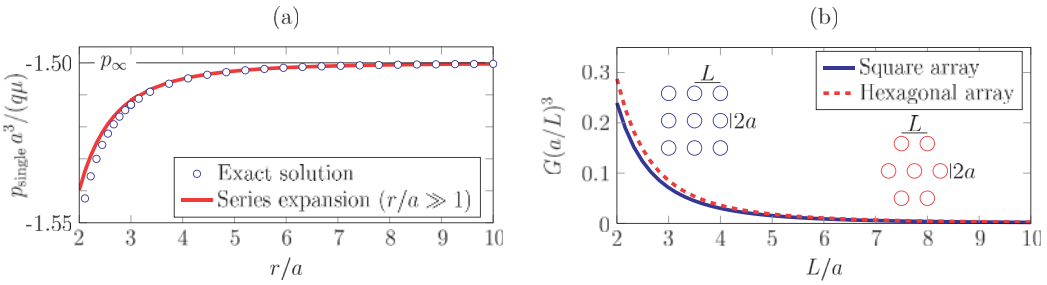


FIG. 5. The influence of hydrodynamics interactions. (a) Plot of the pressure $p_{\text{single}}$ produced by flow through a single pore on the top surface of the filter ($z = 0$). The pressure is a function of the distance $r$ from the pore center, and it approaches the value $p_\infty = -3\mu q/(2a^3)$ from below when $r/a \to \infty$. Results are shown for Sampson's exact solution (Eq. (13), circles) and the power series expansion (Eq. (14), red solid line). (b) Plot of the lowest-order correction $G(a/L)^3$ associated with hydrodynamic interaction effects to Sampson's single-pore result, see Eq. (16). Results are given for pores distributed in a square ($G = 1.9$) and hexagonal ($G = 2.3$) pattern. The correction is a function of the non-dimensional parameter $L/a$, where $L$ denotes the center-to-center shortest distance between pores and $a$ is the pore radius.

$p_{\text{single}}$, as a function of the radial distance $r$ from the center of that pore is[20]

$$p_{\text{single}}(r, z = 0) = \begin{cases} 0 & (r < a) \\ -\frac{3}{\pi}\frac{\mu q}{a^3}\left(\frac{1}{\sinh\zeta} + \tan^{-1}(\sinh\zeta)\right) & (r > a), \end{cases} \tag{13}$$

where $\zeta = \cosh^{-1}\left(\frac{r}{a}\right)$. When written as a power series for $(r/a) \gg 1$, Eq. (13) is

$$p_{\text{single}}(r, z = 0) = -\frac{3\mu q}{a^3}\left[\frac{1}{2} + \frac{1}{3\pi}\left(\frac{a}{r}\right)^3 + \mathcal{O}\left(\left(\frac{a}{r}\right)^4\right)\right]. \tag{14}$$

At large distances from the pore the pressure approaches the value $p_\infty = -3\mu q/(2a^3)$ from below, as shown in Fig. 5. The negative contribution to the pressure thus enhances the volume flux through an adjacent pore. As a first correction to account for the hydrodynamic interaction between the pores, we therefore subtract the value of the pressure produced by each single-pore solution at the center of the other pore ($r = L$). Therefore, the formula for the pressure drop versus flow rate per pore becomes

$$\frac{\Delta p}{q} = \frac{3\mu}{a^3}\left[1 - \frac{2}{3\pi}\left(\frac{a}{L}\right)^3 + h.o.t.\right], \tag{15}$$

where the order of magnitude of higher-order terms (*h.o.t.*) needs to be established by a more detailed argument. The factor of 2 in the $\left(\frac{a}{L}\right)^3$ correction arises from the added pressure of opposite sign but equal magnitude on the lower half plane ($z < 0$).

Equation (15) demonstrates that hydrodynamic interactions decrease the pressure drop required to produce a given flow through a pore or, alternatively, for a given pressure drop, the flow rate per pore is higher than predicted by Sampson's single-pore result. We note that even after subtracting the single-pore pressure produced at the center of the other pore, condition (ii) above is still not satisfied, owing to pressure variations at distances $r \approx L + a$. These pressure variations suggest corrections at least $O(a/L)$ smaller than given in Eq. (15).

### B. An array of pores

To Sampson's $\Delta p/q$ ratio for an isolated pore one must linearly add the hydrodynamic corrections associated with the interaction between that pore and every other pore in the microfilter. The number of pores a given distance away depends on the geometrical arrangement of the pores in the microfilter. The correction is therefore a function of (i) the pattern layout of the pores in the filter and (ii) $L/a$, where $L$ is defined as the shortest distance between pores in that pattern. Thus, in general, we have

$$\frac{\Delta p}{q} \approx \frac{3\mu}{a^3}\left[1 - G\left(\frac{a}{L}\right)^3\right], \tag{16}$$

where $G$ is a constant dependent only on the geometrical layout of the pores in the microfilter. In particular, $G$ is calculated by linearly adding the hydrodynamic interaction corrections between any given pore and all the other pores in the microfilter. For example, for the case where the pattern is a square grid of circular pores, with center-to-center spacing $L$, we find

$$G_{\mathrm{sq}} = \frac{2}{3\pi}\left(\left(4+2^{1/2}\right)\left(\sum_{j=1}^{\infty} j^{-3}\right) + 8\sum_{j=2}^{\infty}\sum_{i=1}^{j-1}\frac{1}{\left(j^2+i^2\right)^{3/2}}\right), \tag{17}$$

where $\sum_{j=1}^{\infty} j^{-3} \approx 1.2$. Therefore, we find $G_{\mathrm{sq}} \approx 1.9$. In addition, for the case of an hexagonal pattern, taking the limit where the pore pattern extends to infinity, $G_{\mathrm{hex}} \approx 2.3$. These limiting results for the cases of infinitely many pores have also been derived via an analytical corrective-iterative procedure by Tio and Sadhal,[18] whereby higher-order corrections were also found. Figure 5 shows the correction to Sampson's base result as a function of $L/a$ for the square and hexagonal patterns.

Typical filters shown in Fig. 1 have values of $L/a$ in the range 3 to 7, thus, in practice, the increase in flow due to the hydrodynamic interactions can change from being negligible to being about 10% of Sampson's isolated pore result.

## V. THE INFLUENCE OF SLIP

A fundamental assumption used when deriving the base case, Eq. (5), is that the flow occurs in the continuum regime, where the Navier-Stokes equations and the no-slip condition at solid boundaries apply. For gas flows, the validity of this approximation is measured by the Knudsen number ($\mathcal{K}_n = \lambda/a$), the non-dimensional ratio of the mean free path $\lambda$ of a molecule in the fluid to the macroscopic characteristic lengthscale of the geometry, e.g., the pore radius $a$.[9,22] For gas flow through microfilters (see, e.g., Yang *et al.*[7]), based on the mean free path of air under standard conditions (≈65 nm), the Knudsen number is $\mathcal{K}_n \approx 0.01 - 0.03$.[7] At these values the dynamics are in the slip-flow regime, $10^{-2} < \mathcal{K}_n < 10^{-1}$, where the Navier-Stokes equations are still valid but they must be supplemented by a slip-flow boundary condition at solid walls.[9,22] In this section, we provide a correction to Eq. (5) to account for slip effects. A similar slip flow boundary condition is applicable to liquid flows at the sub-micron scale when the liquid is adjacent to a solvophobic boundary.[23]

In the slip-flow regime the local tangential velocity $\mathbf{v}_t(\mathbf{x})$ at a solid boundary is proportional to the tangential fluid rate of strain at that point.[22,24,25] Specifically, for gas flows adjacent to solid boundaries

$$\mathbf{v}_t(\mathbf{x}) = \left(\frac{2-\sigma_m}{\sigma_m}\right)\lambda\left[\mathbf{n}\cdot\left(\nabla\mathbf{v}(\mathbf{x}) + (\nabla\mathbf{v}(\mathbf{x}))^T\right)\right]_t. \tag{18}$$

Here, $\sigma_m$ is the tangential momentum accommodation coefficient, whose value depends on wall surface properties, though empirically $\sigma_m \approx 0.9 - 1.0$ for air flow.[9,26] For simplicity, henceforth we assume $\sigma_m = 1$, which corresponds to the case of perfect diffuse reflection of the gas molecules at the wall.[9] Finally, the $[\,\cdot\,]_t$ notation indicates (twice) the tangential component of the fluid strain rate at the wall ($\mathbf{n}$ is the unit normal vector to the wall).

We consider the corrections to the Sampson and Poiseuille pressure drops separately, implicitly assuming that the linear addition of the two terms remains a good approximation. First, a direct calculation shows that in Sampson's solution the tangential stress at the filter walls is zero.[13,20] Thus, Sampson's solution remains valid even under slip and the slip effects correction only affects the Poiseuille flow pressure drop contribution, to which we turn next.

For flow along the pore, we take $r$ as the radial distance from the pore axis and $z$ as the axial coordinate along the flow direction (see Fig. 2(b)), so the slip boundary condition (18) simplifies to

$$v_z\,|_{\mathrm{wall}} = -\lambda\frac{dv_z}{dr}\,|_{\mathrm{wall}}\,. \tag{19}$$

For liquid flows $\lambda$ is referred to as the slip length. Solving the Stokes flow equations (1) with this boundary condition and a pressure drop $\Delta p$ across the pore of thickness $t$ is a standard exercise. The

velocity profile is $v_z(r) = a^2\Delta p/(4\,\mu\,t)\left[(1-(r/a)^2+2\,\lambda/a\right]$ from which we find

$$\frac{\Delta p}{q} = \frac{8\mu}{\pi a^3}\frac{t}{a}\left(\frac{1}{1+4\mathcal{K}_n}\right), \tag{20}$$

where the factor in parenthesis represents the slip correction to the Poiseuille pressure drop. For gas flows, the slip effects decrease the Poiseuille pressure drop required to drive a given flow rate by up to approximately 10% for typical Knudsen numbers mentioned above.

## VI. THE INFLUENCE OF INERTIA

A fundamental approximation used when deriving the basic result (5) was to neglect inertial effects. In this section we discuss how to account for low-Reynolds-number inertial corrections to this result. We do not consider high-Reynolds-number flow here, but refer the reader to Refs. 8 and 28. A general equation relating the pressure drop $\Delta p$, flow rate $q$, viscosity $\mu$, density $\rho$, and pore radius $a$ can be obtained by dimensional analysis following, for example, Bond[29] and Johansen.[27] Since there are only two independent non-dimensional products of the five variables, we can write without loss of generality

$$\frac{\Delta p}{q} = \frac{\mu}{a^3}\phi(\mathcal{R}_e), \tag{21}$$

where $\phi$ is an unknown function of the pore Reynolds number $\mathcal{R}_e = \rho U a/\mu$. Experimental values of $\phi$ can be obtained from the data collected by Johansen[20,27] who flowed lubrication oil through sharp-edged circular orifices situated inside a larger pipe. For low-Reynolds-number flows in these configurations, we are only aware of two experimental papers dating back 80 years.[27,29] As shown in Fig. 6, the prefactor in Eq. (21) determined by Johansen approaches $\phi = 3$ at low Reynolds numbers, in accord with Sampson's prediction in (2). Similar results were found by Bond[29] who reported a prefactor of $\phi = 2.92 \pm 0.05$ in the limit $\mathcal{R}_e \ll 1$. In Fig. 6, for values greater than $\mathcal{R}_e \approx 4$, the prefactor $\phi$ increases linearly with $\mathcal{R}_e$.

To rationalize the dependence $\phi$ on the Reynolds number $\mathcal{R}_e$ observed in Fig. 6 we note that at moderate Reynolds numbers, a significant part of the pressure drop $\Delta p$ is used for accelerating the liquid and thus increasing the kinetic energy of the flow. To estimate this effect we use Bernoulli's equation to approximate the inertial contribution to the total pressure drop[28,30] as

$$\Delta p \approx \frac{3\mu q}{a^3} + \rho u^2. \tag{22}$$

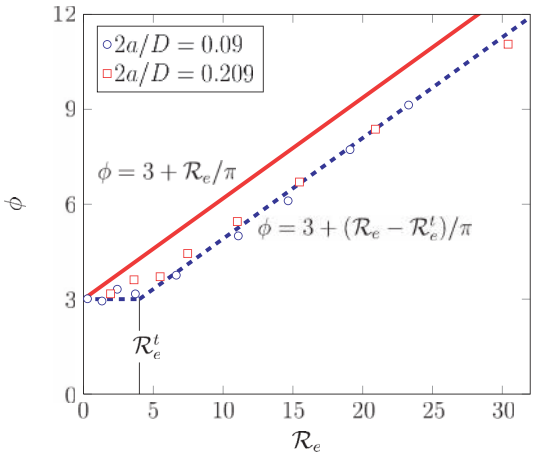


FIG. 6. The prefactor $\phi$ in Eq. (21) plotted as a function of Reynolds number $\mathcal{R}_e$. Experimental data (circles and squares) from Johansen[20,27] (Fig. 13), who flowed lubrication oil through sharp-edged circular orifices of radius $a$ situated inside a larger pipe of diameter $D$. Data shown here were obtained with $2a/D = 0.090$ (circles) and $2a/D = 0.209$ (squares). Lines show the predictions of Eqs. (23) (solid) and (24) (dashed, $\mathcal{R}_e^t = 4$).

Rearranging, the pressure drop per flow rate relation is

$$\frac{\Delta p}{q} \approx \frac{\mu}{a^3}\left[3 + \frac{\mathcal{R}_e}{\pi}\right]. \tag{23}$$

This result corresponds to $\phi(\mathcal{R}_e) = 3 + \mathcal{R}_e/\pi$, which is plotted as a solid line in Fig. 6. While the slope $\mathrm{d}\phi/\mathrm{d}\mathcal{R}_\mathrm{e} = 1/\pi$ is well capture by Eq. (23), the onset of inertial corrections to the pure Sampson flow (i.e., deviations from $\phi = 3$) is seen to occur around a transition Reynolds number $\mathcal{R}_e^t = 4$. Bond, who used thicker pores, found that the transition occurred at $\mathcal{R}_e^t \approx 10$.[29] The precise value of $\mathcal{R}_e^t$ is thus likely to depend on the pore thickness, and on details of the flow and the experimental boundary conditions. From the rough experimental data available, however, $\mathcal{R}_e^t$ observed to approximately coincide with the point where the two contributions to the pressure loss in Eq. (22) are equal, i.e., when $\mathcal{R}_e^t = 3\pi \approx 9.4$. From these considerations, we present an empirical formula for the prefactor $\phi$ in Eq. (21)

$$\phi(\mathcal{R}_e) = 3\left[1 + f(\mathcal{R}_e)\right], \tag{24}$$

where the function $f$ is given by

$$f(\mathcal{R}_e) = \begin{cases} 0 & \mathcal{R}_e < \mathcal{R}_e^t \\ (\mathcal{R}_e - \mathcal{R}_e^t)/(3\pi) & \mathcal{R}_e > \mathcal{R}_e^t. \end{cases} \tag{25}$$

This expression for the prefactor $\phi$ with $\mathcal{R}_e^t = 4$ is plotted as a dashed line in Fig. 6.

We can also discuss briefly the limit $\mathcal{R}_e \ll 1$. In Appendix B we report the calculation of the $\mathcal{O}(\mathcal{R}_e)$ correction to the pressure-drop-flow-rate relation. We use a regular perturbation expansion familiar in low-Reynolds-number flows.[31] In fact, we find there is no $\mathcal{O}(\mathcal{R}_e)$ correction, which suggests the next correction is $\mathcal{O}(\mathcal{R}_e^2)$. This feature is not inconsistent with the small variation in Fig. 6 for $\mathcal{R}_e < 4$.

## VII. DISCUSSION AND CONCLUSIONS

In this article, we have classified the effects that contribute to the hydraulic resistance of a microfilter. Consider first the case of a filter with a regular array of identical circular pores. Combining the different results presented in the article, we find a formula for the pressure drop versus flow rate per pore under the assumptions of incompressibility and low Reynolds numbers

$$\frac{\Delta p}{q} = \frac{3\mu}{a^3}\left[1 - G\left(\frac{a}{L}\right)^3 + \frac{8}{3\pi}\frac{t}{a}\left(\frac{1}{1+4\mathcal{K}_n}\right) + f(\mathcal{R}_e)\right]. \tag{26}$$

The $\mu/a^3$ general scaling form for an infinitely thin plate follows from dimensional analysis. The factor 3 represents the pressure drop associated with Sampson flow through an isolated pore in a plane. The term $-G(a/L)^3$ represents the correction to Sampson's result associated with the hydrodynamic interactions between the flow through different pores, which turns out to increase the flow through the pores at any given pressure drop. The constant $G$ is a geometric factor, dependent on the pattern of pores, e.g., $G_\mathrm{sq} = 1.9$ for a square pattern, $G_\mathrm{hex} = 2.3$ for an hexagonal pattern. The term $8t/(\pi a)$ accounts for the pressure drop due to the Poiseuille flow along the pore axis. This result assumed no-slip at the walls and therefore it is corrected by the factor $1/(1 + 4\mathcal{K}_n)$, where $\mathcal{K}_n$ is the Knudsen number. Finally we found that the correction associated with the presence of inertial effects is given by $f(\mathcal{R}_e)$ in Eq. (25) which we obtained using scaling arguments and comparison to experimental data obtained by Johansen.[27]

If we then account for a distribution of pore radii with probability function $P(a, \boldsymbol{\sigma})$ and focus on the case where hydrodynamic interactions, wall slip, and inertial effects are negligible, then Eq. (5) can be generalized to the average pressure drop per flow rate

$$\left\langle \frac{\Delta p}{q} \right\rangle = \frac{3\mu}{\bar{a}^3}\left[\frac{1}{M_3} + \frac{1}{M_4}\frac{8}{3\pi}\frac{t}{\bar{a}}\right]. \tag{27}$$

Here, $\bar{a}$ is the average pore radius and the factors $M_3$ and $M_4$ are the scaled moments defined in Eq. (11). The moments increase in magnitude with the distribution width, and the factors $M_3$ and

$M_4$ thus quantify by how much the flow rate increases at a given pressure due to the dispersion of radii. As discussed in Appendix A it is straightforward to incorporate the effects of hydrodynamic interactions, wall slip, and inertia in the averaging over pore radii performed in Eq. (8) that leads to (27).

The formulas (26) and (27) allow for accurate design of microfilters for applications such as removal of air- or water-borne particles. The various effects discussed suggest that even slight modifications to pore size and density can have a large impact on the effective hydraulic resistance of the filter. We further note that all the effects considered here appear relatively straightforward to study experimentally in a microfluidic system. It would also be interesting to generalize the results to other pore geometries, for example, by considering fibrous materials.

## ACKNOWLEDGMENTS

We thank N. M. Holbrook and M. Knoblauch for useful discussions. K.H.J. was supported by the Air Force Office of Scientific Research (Award No. FA9550-09-1-0188), the Materials Research Science and Engineering Center at Harvard University (MRSEC, NSF Grant No. DMR-0820484), the Danish Council for Independent Research | Natural Sciences, and the Carlsberg Foundation. A.V. acknowledges the support of the Center for Neuroscience and Cell Biology project (PEst-C/SAU/LA0001/2013-2014) and Portuguese national funds via the programs FEDER and COMPETE, and via Fundação para a Ciência e a Tecnologia and a subsidy of the Russian Government to support the Program of Competitive Growth of Kazan Federal University among World's Leading Academic Centers. H.A.S. thanks the NSF for support via Grant No. CBET-1234500.

## APPENDIX A: THE INFLUENCE OF HYDRODYNAMIC INTERACTIONS BETWEEN PORES OF DIFFERENT SIZE

We consider the hydrodynamic interaction between a pore of radius $a_i$ and the neighboring pores in an infinitely thin plane. We assume that the pore radii follow a probability function $P(a, \boldsymbol{\sigma})$ as discussed in Sec. III. For simplicity we first assume that pore $i$ only interacts with the $n$ nearest pores located a distances $L$ away from the centre of pore $i$. It is possible to consider longer range interactions and distributions of $L$ but we shall not do that here.

The pressure drop per flow rate for pore $i$ in the presence of neighboring pores can be written as

$$\frac{\Delta p + \delta p}{q_i} = \frac{3\mu}{H_i}, \tag{A1}$$

where

$$\frac{1}{H_i} = \frac{1}{a_i^3}\left[1 + \frac{8}{3\pi}\frac{t}{a_i}\left(\frac{1}{1+4\mathcal{K}_{n,i}}\right) + f(\mathcal{R}_{e,i})\right] \tag{A2}$$

and $\delta p$ is the additional pressure drop due to hydrodynamic interactions. As discussed in the text leading to Eq. (15), the change in the pressure drop due to one neighbor is $2\mu q/(\pi r^3)$, where $r$ is the distance between the two interacting pores. Taking into account the nearest $n$ neighbors leads to

$$\delta p = \frac{2}{\pi}\frac{\mu}{L^3}\sum_{j=1}^{n} q_j = \frac{2}{3\pi}\frac{\Delta p}{L^3}\sum_{j=1}^{n} H_j. \tag{A3}$$

We evaluate the sums over the radii by taking the statistical average of $H$ following Eq. (7)

$$\delta p = \frac{2n}{3\pi}\frac{\langle H\rangle}{L^3}\Delta p. \tag{A4}$$

Using Eq. (A4) in Eq. (A1) and taking the expectation value of $q$ leads to

$$\langle q\rangle = \frac{\langle H\rangle}{3\mu}\left[1 + \frac{2n}{3\pi}\frac{\langle H\rangle}{L^3}\right]\Delta p. \tag{A5}$$

Equation (A5) finally allows us to determine the ratio of pressure drop to flow rate

$$\left\langle \frac{\Delta p}{q} \right\rangle \approx \frac{3\mu}{\langle H \rangle} \left[ 1 - \frac{2n}{3\pi} \frac{\langle H \rangle}{L^3} \right]. \tag{A6}$$

Equation (A6) has the same form as (16) and we identify $2n/(3\pi)$ as the geometric factor $G$ discussed in Sec. IV B. For the square array we can approximate $n = 8$ which yields $G \approx 1.7$ in rough accord with the value $G_{\text{sq}} = 1.9$ obtained from Eq. (17).

## APPENDIX B: THE INFLUENCE OF INERTIA

In this Appendix we argue that the low Reynolds number inertial correction to Eq. (5) scales as $\mathcal{R}_e^2$. Since it is not clear that one may simply linearly add separate inertial corrections to the Sampson and the Poiseuille flow results, let us address the full microfilter geometry, that is, we consider both the Sampson pore-in-a-plane geometry and the axial pore channel geometry as a single problem. To include inertial effects, we begin with the full Navier-Stokes equations. Non-dimensionalizing lengths by $\tilde{\mathbf{x}} = \mathbf{x}/a$, pressure by $\tilde{p} = p/\Delta p$, and velocities by $\tilde{\mathbf{v}} = \mathbf{v}/(\Delta p a/\mu)$, the Reynolds number is defined as $\mathcal{R}_e = \Delta P a^2 \rho/\mu^2$, and the steady incompressible Navier-Stokes equations become

$$\nabla^2 \tilde{\mathbf{v}} - \nabla \tilde{p} = \mathcal{R}_e (\tilde{\mathbf{v}} \cdot \nabla \tilde{\mathbf{v}}), \tag{B1a}$$

$$\nabla \cdot \tilde{\mathbf{v}} = 0. \tag{B1b}$$

These equations are subject to the boundary conditions $\tilde{\mathbf{v}} \to 0$ and $\tilde{p} \to \pm 1/2$ as $|\tilde{\mathbf{x}}| \to \mp\infty$ and $\tilde{\mathbf{v}} = \mathbf{0}$ at the filter walls. Let us denote the exact solution to Stokes equations in this non-dimensional formulation of the problem by $(\tilde{\mathbf{v}}_0, \tilde{p}_0)$. Because of mass conservation the velocity at $\pm\infty$ decays as $1/|\tilde{\mathbf{x}}|^2$ and consequently the Stokes solution is uniformly valid everywhere, i.e., as $\mathcal{R}_e \to 0$, the relative size of the inertial term compared to the other two terms goes to zero, uniformly, everywhere in space. Therefore we conclude that the problem admits a regular perturbation expansion[31]

$$\tilde{\mathbf{v}} = \tilde{\mathbf{v}}_0 + \mathcal{R}_e \tilde{\mathbf{v}}_1 + \mathcal{R}_e^2 \tilde{\mathbf{v}}_2 + \mathcal{O}(\mathcal{R}_e^3), \tag{B2a}$$

$$\tilde{p} = \tilde{\mathbf{v}}_0 + \mathcal{R}_e \tilde{p}_1 + \mathcal{R}_e^2 \tilde{p}_2 + \mathcal{O}(\mathcal{R}_e^3). \tag{B2b}$$

Symmetry arguments will now suffice to show that the flow rate through the pore associated with the $\tilde{\mathbf{v}}_1$ velocity field must be zero. Substituting (B2a) and (B2b) into (B1a) and equating terms order by order in $\mathcal{R}_e$, yields at order 1 the equations

$$\nabla^2 \tilde{\mathbf{v}}_1 - \nabla \tilde{p}_1 = \tilde{\mathbf{v}}_0 \cdot \nabla \tilde{\mathbf{v}}_0 \qquad \nabla \cdot \tilde{\mathbf{v}}_1 = 0. \tag{B3}$$

The symmetry of the geometry, the symmetry of the Stokes equations, and the symmetry of the boundary conditions imply that the Stokes solution $(\tilde{\mathbf{v}}_0, \tilde{p}_0)$ is anti-symmetric about the $\tilde{z} = 0$ plane

$$\tilde{\mathbf{v}}_0(\tilde{r}, \tilde{z}) = (-v_{0\tilde{r}}(\tilde{r}, -\tilde{z}), v_{0\tilde{z}}(\tilde{r}, \tilde{z}))\,, \tag{B4a}$$

$$\tilde{p}_0(\tilde{r}, \tilde{z}) = -\tilde{p}_0(\tilde{r}, \tilde{z}), \tag{B4b}$$

where the subscripts indicate the corresponding velocity components. Therefore the term $\tilde{\mathbf{v}}_0 \cdot \nabla \tilde{\mathbf{v}}_0$ satisfies the symmetry

$$(\tilde{\mathbf{v}}_0 \cdot \nabla \tilde{\mathbf{v}}_0)(\tilde{r}, \tilde{z}) = ((\tilde{\mathbf{v}}_0 \cdot \nabla \tilde{\mathbf{v}}_0)_{\tilde{r}}(\tilde{r}, -\tilde{z}), -(\tilde{\mathbf{v}}_0 \cdot \nabla \tilde{\mathbf{v}}_0)_{\tilde{z}}(\tilde{r}, -\tilde{z}))\,. \tag{B5}$$

Based on this symmetry of the inertial term (B5), the symmetry of Eq. (B3) and the homogeneity of the boundary conditions that $(\tilde{\mathbf{v}}_1, \tilde{p}_1)$ satisfies (both $\tilde{\mathbf{v}}_1$ and $\tilde{p}_1$ go to zero at $\pm\infty$), we conclude that

$$\tilde{\mathbf{v}}_1(\tilde{r}, \tilde{z}) = (\tilde{v}_{1\tilde{r}}(\tilde{r}, -\tilde{z}), -\tilde{v}_{1\tilde{z}}(\tilde{r}, -\tilde{z}))\,. \tag{B6}$$

This result implies that $\tilde{\mathbf{v}}_1$ at $\tilde{z} = 0$ does not have a vertical component and thus there is no flow across the pore associated with the $\tilde{\mathbf{v}}_1$ velocity field. A similar assertion, however, cannot be made

concerning $\tilde{\mathbf{v}}_2$. This time, defining $\mathbf{A} \equiv \tilde{\mathbf{v}}_0 \cdot \nabla \tilde{\mathbf{v}}_1 + \tilde{\mathbf{v}}_1 \cdot \nabla \tilde{\mathbf{v}}_0$ for notational simplicity, we have

$$\mathbf{A}(\tilde{r}, \tilde{z}) = (-A_{\tilde{r}}(\tilde{r}, -\tilde{z}), A_{\tilde{z}}(\tilde{r}, -\tilde{z})), \tag{B7}$$

and the symmetry of $\tilde{\mathbf{v}}_2$ is of the form

$$\tilde{\mathbf{v}}_2(\tilde{r}, \tilde{z}) = (-\tilde{v}_{2\tilde{r}}(\tilde{r}, -\tilde{z}), \tilde{v}_{2\tilde{z}}(\tilde{r}, -\tilde{z})), \tag{B8}$$

hence, we cannot assert that $\tilde{\mathbf{v}}_2$ has no vertical component at $z = 0$.

In dimensional form, we can therefore write the asymptotic correction to Eq. (5) that accounts for inertial effects as

$$\frac{\Delta p}{q} = \frac{3\mu}{a^3}\left(\left[1 + \frac{8}{3\pi}\frac{t}{a}\right] + \mathcal{O}(\mathcal{R}_e^2)\right). \tag{B9}$$


[1] L. A. Spielman, "Particle capture from low-speed laminar flows," Annu. Rev. Fluid Mech. **9**, 297–319 (1977).
[2] H. Wyss, D. Blair, J. Morris, H. A. Stone, and D. Weitz, "Mechanism for clogging of microchannels," Phys. Rev. E **74**, 061402 (2006).
[3] J. Lin, D. Bourrier, M. Dilhan, and P. Duru, "Particle deposition onto a microsieve," Phys. Fluids **21**, 073301 (2009).
[4] M. T. Tyree, M. H. Zimmermann, and M. H. Zimmermann, *Xylem Structure and the Ascent of Sap* (Springer, New York, 2002).
[5] K. H. Jensen, D. L. Mullendore, N. M. Holbrook, T. Bohr, M. Knoblauch, and H. Bruus, "Modeling the hydrodynamics of phloem sieve plates," Front. Plant Sci. **3**, 151 (2012).
[6] S. Gravelle, L. Joly, F. Detcheverry, C. Ybert, C. Cottin-Bizonne, and L. Bocquet, "Optimizing water permeability through the hourglass shape of aquaporins," PNAS **110**, 16367–16372 (2013).
[7] X. Yang, J. M. Yang, Y.-C. Tai, and C.-M. Ho, "Micromachined membrane particle filters," Sens. Actuators **73**, 184–191 (1999).
[8] D. J. Tritton, *Physical Fluid Dynamics*, 2nd ed. (Oxford University Press, New York, 1988).
[9] I. Ahmed and A. Beskok, "Rarefaction, compressibility, and viscous heating in gas microfilters," J. Thermophys. Heat Transfer **16**, 161–170 (2002).
[10] H. Y. Yang, Z. J. Han, S. F. Yu, K. L. Pey, K. Ostrikov, and R. Karnik, "Carbon nanotube membranes with ultrahigh specific adsorption capacity for water desalination and purification," Nat. Commun. **4**, 2220 (2013).
[11] D. L. Mullendore, C. W. Windt, H. Van As, and M. Knoblauch, "Sieve tube geometry in relation to phloem flow," Plant Cell **22**, 579–593 (2010).
[12] M. M. Couette, "Etudes sur le frottement des liquides," Ann. Chim. Phys. **21**, 433–510 (1890).
[13] R. A. Sampson, "On Stokes's current function," Philos. Trans. R. Soc. London, Ser. A **182**, 449–518 (1891).
[14] R. Roscoe, "The flow of viscous fluids round plane obstacles," Philos. Mag. **40**, 338–351 (1949).
[15] H. L. Weissberg, "End correction for slow viscous flow through long tubes," Phys. Fluids **5**, 1033 (1962).
[16] Z. Dagan, S. Weinbaum, and R. Pfeffer, "An infinite-series solution for the creeping motion through an orifice of finite length," J. Fluid Mech. **115**, 505–523 (1982).
[17] H. Hasimoto, "On the flow of a viscous fluid past a thin screen at small Reynolds numbers," J. Phys. Soc. Jpn. **13**, 633–639 (1958).
[18] K.-K. Tio and S. S. Sadhal, "Boundary conditions for Stokes flows near a porous membrane," Appl. Sci. Res. **52**, 1–20 (1994).
[19] C. Y. Wang, "Stokes flow through a thin screen with patterned holes," AIChE J. **40**, 419–423 (1994).
[20] J. Happel and H. Brenner, *Low Reynolds Number Hydrodynamics* (Springer, Hingham, MA, USA, 1983).
[21] V. K. Rohatgi, *An Introduction to Probability Theory and Mathematical Statistics* (Wiley, New York, 1976).
[22] S. A. Schaaf and P. L. Chambre, *Flow of Rarefied Gases* (Princeton University Press, 1961).
[23] E. Lauga and H. A. Stone, "Effective slip in pressure-driven Stokes flow," J. Fluid Mech. **489**, 55–77 (2003).
[24] J. C. Maxwell, "On stresses in rarified gases arising from inequalities of temperature," Philos. Trans. R. Soc. London **170**, 231–256 (1879).
[25] A. B. Basset, *A Treatise on Hydrodynamics with Numerous Examples* (Dover, New York, 1961).
[26] A. K. Sreekanth, "Slip flow through long circular tubes," in *Rarefied Gas Dynamics*, edited by L. Trilling and H. Y. Wachman (Academic Press, New York, 1968), pp. 667–680.
[27] F. C. Johansen, "Flow through pipe orifices at low Reynolds numbers," Proc. R. Soc. A **126**, 231–245 (1930).
[28] O. G. Tietjens and L. Prandtl, *Applied Hydro- and Aeromechanics* (Dover, New York, 1957).
[29] W. N. Bond, "Viscosity determination by means of orifices and short tubes," Proc. Phys. Soc. London **34**, 139 (1921).
[30] S. Goldstein, *Modern Developments in Fluid Dynamics* (Dover, New York, 1965).
[31] L. G. Leal, *Laminar Flow and Convective Transport Processes* (Butterworth-Heinemann, Boston, 1992).